Analytical solution for the lubrication force between two spheres in a bi-viscous fluid

A. Vázquez-Quesada[1, a)] and M. Ellero[1, b)]

Zienkiewicz Centre for Computational Engineering (ZCCE),
Swansea University, Bay Campus, Swansea SA1 8QQ,
United Kingdom.
Tel.: +44 (1792) 295514

An analytical solution for the calculation of the normal lubrication force acting between two moving spheres embedded in a shear-thinning fluid represented by a bi-viscous model is provided. The resulting force between the suspended spheres exhibits a consistent transition between the Newtonian constant-viscosity limits and it reduces to the well-know standard Newtonian lubrication theory for viscosity-ratio approaching one. Effects of several physical parameters of the theory are analyzed under relevant physical conditions, i.e. for a prototypical case of two non-colloidal spheres immersed in a non-Newtonian fluid with rheology parameterized by a bi-viscosity model. Topological results for high/low-viscosity regions in the gap between spheres are also analyzed in detail showing a rich phenomenology. The presented model enables the extension of lubrication dynamics for suspensions interacting with non-Newtonian matrices and provides a clean theoretical framework for new numerical computations of flow of dense complex particulate systems.

[a)]Electronic mail: A.Vazquez-Quesada@swansea.ac.uk

[b)]Electronic mail: M.Ellero@swansea.ac.uk

I. INTRODUCTION

Particulate suspensions are ubiquitous in nature and industrial applications, and the understanding of their flow properties represents therefore a challenging academic and relevant technical problem[1,2]. Although the dilute and semidilute rheological behaviors for suspension with a Newtonian matrix are well understood[3–6], when the solid concentration becomes sufficiently large many new issues arise[7,8]. In very dense systems, particles under flow can get very close to each other, entering the so-called lubrication regime. From a computational perspective, reproducing correctly the lubrication force acting between two particles within a very thin separation gap is a very challenging task: when direct numerical simulations (DNS) are considered, correct description of the lubrication is possible only at the price of a significant increase of the numerical resolution in the gap and therefore CPU resources. Although this approach has been frequently adopted[9,10], it appears to be limited in its application to systems with a small number of suspended particles, whereas realistic large-scale dense systems - with multiple near-contact lubrication-interactions - are out of the current DNS capabilities. In order to bypass some of these technical issues, simulations are usually performed by separating long-range hydrodynamics interactions between particles - obtained conventionally from explicit-solvent[11,12] or implicit-solvent models[13] - from the short-range hydrodynamic interactions which are instead taken into account resorting to exact analytical solutions for the squeezing Stokes flow between close spheres. In the case of simple Newtonian solvents, this framework has been further developed in recent years in order to integrate efficiently the resulting equations of motion and speed-up the simulations[14,15], with the result that systems containing thousands of fully lubricated particles are becoming accessible[16].

On the other hand, the non-Newtonian nature of real suspending media increases significantly the complexity of the lubrication problem. Note that non-Newtonian matrices characterized, for example, by non-constant shear-viscosity, presence of normal stresses or viscoelastic memory effects are not restricted to the flow of complex fluids, e.g. polymer suspensions, melts, emulsions, micelles etc., but might include also so-called 'simple' fluids where complex rheology is still expected, though under extreme flow conditions[17]. It is therefore important to generalize current analytical results for interparticle lubrication forces, in order to incorporate also non-Newtonian matrix effects and target complex par-

ticulate systems[18].

Although the problem of nearly touching spheres in a Newtonian solvent has been widely studied[19–28], there is a scarce number of analytical works focusing on this geometry for a non-Newtonian liquid. In Rodin[29] an asymptotic solution was found for the lubrication force between spheres suspended in a power-law fluid. The final set of equations, however, was obtained in terms of the β function which, in general, needs numerical evaluation. Moreover, the model predicted the presence of an unphysical force singularity for coefficients of the power-law fluid equal to 1/3. Such a behavior was corrected later on by a semi-analytical approximation in Lian *et al.*[30] using a Gaussian integration.

For the case of the tangential lubrication force between spheres in a power-law fluid, an analytical solution is given in Huang *et al.*[31] which, however, diverges for shear thinning solvents, being physically finite only for power-law fluids with exponents larger than one. The authors suggest that such a divergent behavior is caused because the contribution to the force of the outer regions of the gap can not be neglected. On the other hand, numerical solutions have been reported for the case of two close interacting spheres suspended in Herschel-Bulkley fluid[32], power-law fluid with slip boundary conditions[33] or Bingham liquids[34].

In this work we present a fully analytical solution of the normal lubrication force acting between two spheres moving through a non-Newtonian fluid described by the so-called *bi-viscosity model*. This was originally introduced[35,36] to model viscoplastic fluids, i.e. systems characterized by the existence of a yield stress such as toothpaste, paint or several food products[37–39], with a purely viscous regularisation. It can however be used to approximate also the high shear-rate non-Newtonian behavior of many 'simple' fluids such as oil lubricants or other low-molecular weight silicone liquids[40–42], where the viscosity exhibits a physical Newtonian plateau up to very large shear rates, followed by a sudden significant viscous drop. The shear viscosity η of a bi-viscous fluid model reads

$$\eta = \begin{cases} \eta_0, & \text{if } |\dot{\gamma}| < \dot{\gamma}_c \\ \\ \eta_1, & \text{if } |\dot{\gamma}| \geq \dot{\gamma}_c \end{cases} \tag{1}$$

where typically $\eta_1 < \eta_0$ and $\dot{\gamma}_c$ is a critical shear rate parameter. $|\dot{\gamma}| = [\frac{1}{2}(\dot{\boldsymbol{\gamma}} : \dot{\boldsymbol{\gamma}})]^{1/2}$ is the magnitude of the local symmetrized shear rate tensor. Although the rheology of the solvent is relatively simple, a very rich phenomenology emerges in the context of inter-particle

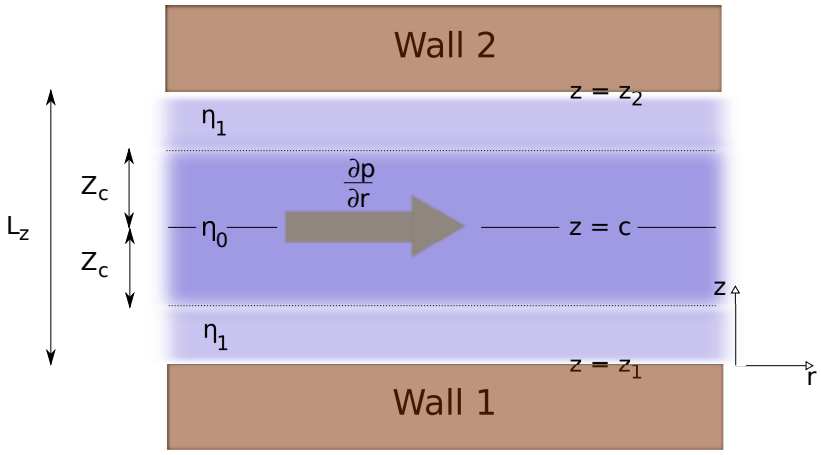

FIG. 1. Scheme of the problem of a bilayer fluid under a pressure gradient between two planar walls.

lubrication.

The paper is structured as follows: in Sec. II, as a corollary the preliminary result for the flow of a bi-viscous fluid driven by a constant pressure gradient between two parallel plates is discussed. This result is generalized in Sec. III, where the calculation of the normal lubrication force between two spheres in a bi-viscous fluid is presented. In order to study the effect of the different physical parameters on the calculated force, we consider a realistic case of non-colloidal spherical particles suspended in polydimethylsiloxane-liquids in Sec. IV. Effect of relative particle velocity, viscosity ratio η_1/η_0 as well as choice of shear rate $\dot{\gamma}_c$ are explored and the results discussed in Sec. IV A and Sec. IV B. In Sec. IV C the local topology of the regions with different viscosities is analyzed. Finally conclusions are provided in Sec. V.

II. SOLUTION OF A BI-VISCOUS FLUID UNDER A PRESSURE GRADIENT BETWEEN TWO PLANAR WALLS

Let us consider first two separate fluids with different viscosities η_0 and η_1 defined between two planar walls located at a distance L_z. We will consider the system of reference $\{r, z\}$ as it is shown in Fig. 1. The bottom and top walls are at the positions $z = z_1$ and $z = z_2$ respectively. The center of the channel is at $z = c = (z_1 + z_2)/2$. The fluid with viscosity

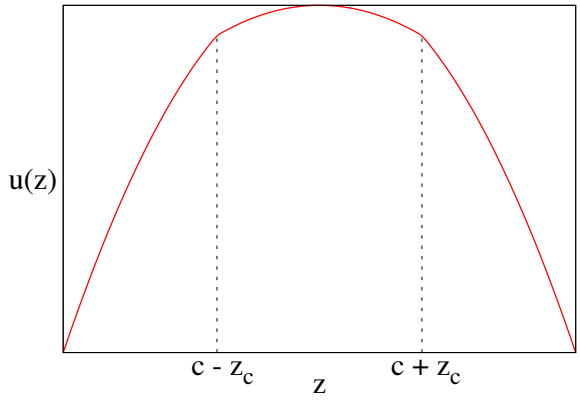

FIG. 2. Velocity profile of a bilayer fluid between two parallel walls.

η_0 is located in the region $|z-c| < z_c$ whereas the fluid with viscosity η_1 is in the region $|z-c| \geq z_c$. We assume that a pressure gradient $\partial p/\partial r$ is applied in the direction r, driving the flow.

If the velocity of the fluid is considered to depend only on the coordinate z, the stationary Navier-Stokes equations for the different layers with viscosities η_0 and η_1 are respectively given by

$$\begin{aligned} \frac{\eta_0}{\rho}\frac{\partial^2}{\partial z^2}u_0 &= \frac{1}{\rho}\frac{\partial p}{\partial r} \\ \frac{\eta_1}{\rho}\frac{\partial^2}{\partial z^2}u_1 &= \frac{1}{\rho}\frac{\partial p}{\partial r} \end{aligned} \tag{2}$$

where ρ is the density and u_0 and u_1 are the velocities in the r direction for the fluids with viscosities η_0 and η_1 respectively. The integration of these equations together with the conditions for the continuity of the velocity field along z, i.e.

$$\begin{aligned} u_1(z_1) = u_1(z_2) &= 0 \\ u_0(c-z_c) &= u_1(c-z_c) \\ u_0(c+z_c) &= u_1(c+z_c) \end{aligned} \tag{3}$$

lead us to the following solution

$$\begin{aligned} u_0(z) &= \frac{1}{2\eta_0}\frac{\partial p}{\partial r}\left[(z-c)^2 - z_c^2\right] + \frac{1}{2\eta_1}\frac{\partial p}{\partial r}\left[z_c^2 - L_z^2/4\right] \\ u_1(z) &= \frac{1}{2\eta_1}\frac{\partial p}{\partial r}(z-z_1)(z-z_2). \end{aligned} \tag{4}$$

Note that the condition of continuity of the stress is also held given that

$$\eta_0\frac{\partial u_0(c\pm z_c)}{\partial z} = \eta_1\frac{\partial u_1(c\pm z_c)}{\partial z} \tag{5}$$

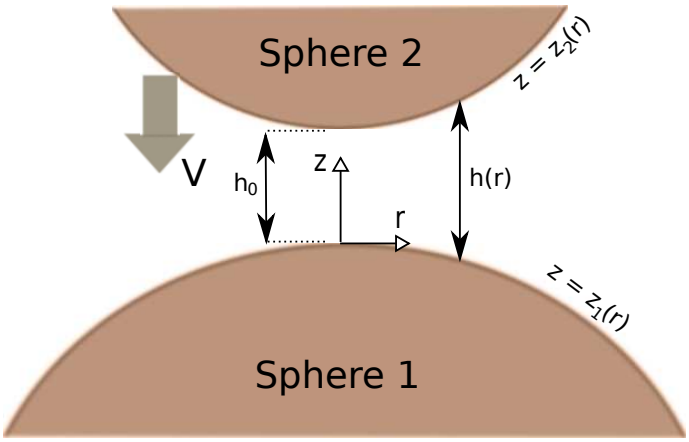

FIG. 3. Scheme of the problem of lubrication between two spheres.

The typical velocity profile of such a system is depicted in the Fig. 2.

If we now consider a single fluid which variable viscosity, i.e. depending on the applied shear rate as defined in Eq. (1), we obtain a similar velocity profile where the distance z_c, however, does depend now on $\dot{\gamma}_c$. The local shear rate of a Newtonian fluid of viscosity η_0 in such a system is given by

$$\dot{\gamma}_0(z) = \frac{1}{\eta_0}\frac{\partial p}{\partial r}(z - c) \tag{6}$$

thus, if we suppose that $\eta_1 < \eta_0$, given that $\dot{\gamma}_0(z) < \dot{\gamma}_1(z)$, we can calculate z_c as

$$z_c = \dot{\gamma}_c \frac{\eta_0}{|\partial p/\partial r|} \tag{7}$$

(note that z_c is not a coordinate, but a distance). Of course, if $z_c > L_z/2$ we should just consider a Newtonian fluid with single viscosity η_0.

III. NORMAL LUBRICATION FORCE BETWEEN TWO SPHERES IN A BI-VISCOUS FLUID

Let us consider now the squeezing flow of two very close spheres of radius a_1 and a_2 immersed in a bi-viscous model fluid with rheology defined by Eq. (1). The normal relative velocity between the spheres is V. The system of reference and the different parameters of the problem are summarized in Fig. 3.

If we consider only small gaps between spheres, their surfaces can be approximated by paraboloids, thus the distance between them can be defined as $h(r) = h_0\left(1 + \frac{r^2}{2ah_0}\right)$, where

$\frac{1}{a} = \frac{1}{a_1} + \frac{1}{a_2}$ and h_0 is the distance between surfaces at $r = 0$[43]. The value of z_c depends now on r and is given by

$$z_c(r) = -\frac{\dot{\gamma}_c \eta_0}{\frac{\partial p}{\partial r}(r)} \tag{8}$$

where we have assumed that the pressure gradient, whose formal expression still needs to be determined, is negative. As in the lubrication force calculation between two spheres in a Newtonian fluid[43], we can consider that the squeezing fluid is moving uni-directionally along the r coordinate if the velocity V is sufficiently small. Depending on the value of the pressure gradient at a given position r, the fluid can behaves either as Newtonian ("mono-viscosity") or non-Newtonian ("bi-viscosity"). The velocity profile is given then by

$$u(r,z) = \begin{cases} u(r,z)|_m, & \text{if } r \in \mathcal{R}_m \\ \\ u(r,z)|_b, & \text{if } r \in \mathcal{R}_b \end{cases} \tag{9}$$

where $\mathcal{R}_m$ is the region of the space where the fluid is mono-viscous, and $\mathcal{R}_b$ where it is bi-viscous. The use of m and b subscripts will be used along this work with the meaning defined in the equation above.

The expressions of the velocity in such a regions are therefore given by

$$u(r,z)|_m = \frac{1}{2\eta_0}\frac{\partial p}{\partial r}(z - z_1(r))(z - z_2(r)) \tag{10}$$

$$u(r,z)|_b = \begin{cases} \frac{1}{2\eta_0}\frac{\partial p}{\partial r}\left[(z - c(r))^2 - z_c^2(r)\right] + \frac{1}{2\eta_1}\frac{\partial p}{\partial r}\left[z_c^2(r) - h^2(r)/4\right], & \text{if } |z - c(r)| < z_c(r) \\ \\ \frac{1}{2\eta_1}\frac{\partial p}{\partial r}(z - z_1(r))(z - z_2(r)), & \text{if } |z - c(r)| \geq z_c(r) \end{cases}$$

Note that now the quantities z_1, z_2 and c generally depend on the r coordinate. For the shake of simplicity, the dependency of $\partial p/\partial r$ on r has not been explicitly written.

The pressure gradient can be calculated by using the mass conservation law, which is written in the coordinates r in the region $\mathcal{R}_m$ as

$$\pi r^2 V \Big|_m = 2\pi r \int_{z_1(r)}^{z_2(r)} u(r,z) dz = -\frac{\pi r}{6\eta_0} \left.\frac{\partial p}{\partial r}\right|_m h^3(r) \tag{11}$$

Thus, the pressure gradient within the region $\mathcal{R}_m$ derives from the last equation as

$$\left.\frac{\partial p}{\partial r}(r)\right|_m = -\frac{6\eta_0 r V}{h^3(r)} \tag{12}$$

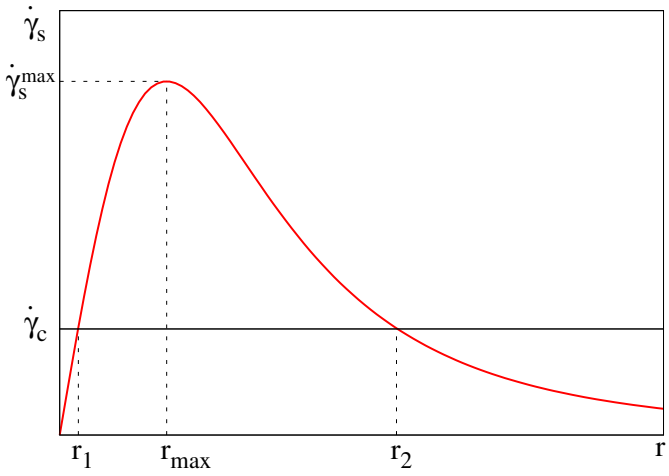

FIG. 4. The maximum shear rate $\dot{\gamma}_s(r)$ depending on r of a Newtonian fluid. The pressure gradient of the fluid will be different than the Newtonian one in the region $r_1 < r < r_2$.

The maximum shear rate $\dot{\gamma}_s$ for a given position r is located at the surfaces of the spheres, and it is given by

$$\dot{\gamma}_s(r) = \frac{-1}{\eta_0}\frac{\partial p}{\partial r}(r)\bigg|_m \frac{h(r)}{2} = \frac{3rV}{h^2(r)} \tag{13}$$

This function, which has been drawn in Fig. 4, is characterized by a maximum at the position

$$r_{max} = \sqrt{\frac{2}{3}ah_0} \tag{14}$$

and its value is given by

$$\dot{\gamma}_s^{max} \equiv \dot{\gamma}_s(r_{max}) = \frac{9}{8}\frac{V}{h_0}\sqrt{\frac{3}{2}\frac{a}{h_0}} \tag{15}$$

Therefore, the condition to obtain a bi-viscosity behavior at some coordinate r is generally defined as

$$\dot{\gamma}_c < \dot{\gamma}_s^{max} \tag{16}$$

If this condition holds, from the $\dot{\gamma}_s(r)$ graph in the Fig. 4, we can conclude that the region $\mathcal{R}_b$ would be located between the two r coordinates r_1 and r_2 (with $r_1 < r_2$). Regions $\mathcal{R}_m$ and $\mathcal{R}_b$ can then be defined as

$$\begin{aligned} r \in \mathcal{R}_m \quad &\text{if} \quad r \leq r_1 \quad \text{or} \quad r \geq r_2 \\ r \in \mathcal{R}_b \quad &\text{if} \quad r_1 < r < r_2 \end{aligned} \tag{17}$$

The conservation of mass applied to the region $\mathcal{R}_b$ allows us to obtain $\partial p/\partial r(r)|_b$.

$$\pi r^2 V\,\big|_b = 2\pi r \int_{z_1(r)}^{z_2(r)} u(r,z)|_b\, dz = -\frac{\pi r}{6\eta_1}\,\frac{\partial p}{\partial r}(r)\,\Big|_b\, h^3(r) + \frac{4\pi r}{3}\,\frac{\partial p}{\partial r}(r)\,\Big|_b\, z_c^3(r)\left(\frac{1}{\eta_1}-\frac{1}{\eta_0}\right) \tag{18}$$

Using Eq. (8) and (13) we can write the last expression in terms of $z_c(r)$ as

$$0 = \left(1-\frac{\eta_1}{\eta_0}\right)\left(\frac{2z_c(r)}{h(r)}\right)^3 + \frac{\eta_1}{\eta_0}\frac{\dot\gamma_s(r)}{\dot\gamma_c}\left(\frac{2z_c(r)}{h(r)}\right) - 1 \tag{19}$$

whose exact solution can be calculated with the Cardano's method: given that the quadratic term is null, the unique real solution to the equation is given by

$$\left(\frac{2z_c(r)}{h(r)}\right) = S_1(r) + S_2(r) \tag{20}$$

$$S_1(r) = \sqrt[3]{\frac{\eta_0}{2(\eta_0-\eta_1)}\left(1+\sqrt{1+\frac{4}{27}\frac{\eta_1^2}{\eta_0^2}\frac{\eta_1}{\eta_0-\eta_1}\left(\frac{\dot\gamma_s(r)}{\dot\gamma_c}\right)^3}\right)}$$

$$S_2(r) = \sqrt[3]{\frac{\eta_0}{2(\eta_0-\eta_1)}\left(1-\sqrt{1+\frac{4}{27}\frac{\eta_1^2}{\eta_0^2}\frac{\eta_1}{\eta_0-\eta_1}\left(\frac{\dot\gamma_s(r)}{\dot\gamma_c}\right)^3}\right)}$$

From this equation we can calculate, with the help of Eq. (8), the expression for the pressure gradient $\partial p/\partial r$, but the result is very difficult to integrate analytically. Without any physical assumption about the value of $\dot\gamma_c$ - which would limit significantly the range of applications of the final formula - we have not found any regime of parameters allowing us to simplify (19) or its solution through series expansion. Instead, given that the cubic polynomial associated to (19)

$$A(x) = \left(1-\frac{\eta_1}{\eta_0}\right)x^3 + \frac{\eta_1}{\eta_0}\frac{\dot\gamma_s(r)}{\dot\gamma_c}x - 1 \tag{21}$$

does not have any extremes, we can consider that the structure of such a function is simple enough to be approximated by a linear interpolation through the points $(x, A(x)) = (0, A(0)), (1, A(1))$, in such a way that the equation to solve now is

$$0 \approx \left(1-\frac{\eta_1}{\eta_0}\left(1-\frac{\dot\gamma_s(r)}{\dot\gamma_c}\right)\right)\left(\frac{2z_c(r)}{h(r)}\right) - 1 \tag{22}$$

whose solution reads

$$\left(\frac{2z_c(r)}{h(r)}\right) \approx \frac{\eta_0}{\eta_0-\eta_1\left(1-\frac{\dot\gamma_s(r)}{\dot\gamma_c}\right)} \tag{23}$$

Note that the linear interpolation which leads to Eq. (22) is equivalent to approximate the cubic term of Eq. (21) as $x^3 \sim x$. From Eq. (8) the pressure gradient is therefore obtained as

$$\frac{\partial p}{\partial r}(r)\bigg|_b \approx -2\dot{\gamma}_c\left(\eta_0-\eta_1\right)h^{-1}(r) - 6\eta_1 V r h^{-3}(r) \tag{24}$$

As a next step, in order to obtain the pressure in a position r, we should integrate the pressure gradient as

$$p(r) = -\int_r^\infty \frac{\partial p}{\partial r}(r)dr \tag{25}$$

which gives an expression which is multiply defined depending on the value of r, i.e.

$$\begin{aligned} p(r)|_{r<r_1} = &-\int_r^{r_1}\frac{\partial p}{\partial r}(r)\bigg|_m dr - \int_{r_1}^{r_2}\frac{\partial p}{\partial r}(r)\bigg|_b dr - \int_{r_2}^{\infty}\frac{\partial p}{\partial r}(r)\bigg|_m dr = \\ &3Va\left[\eta_0 h^{-2}(r) + (\eta_0-\eta_1)\left(h^{-2}(r_2)-h^{-2}(r_1)\right)\right] + \\ &2\dot{\gamma}_c(\eta_0-\eta_1)\sqrt{\frac{2a}{h_0}}\left(\arctan\left(\frac{r_2}{\sqrt{2ah_0}}\right) - \arctan\left(\frac{r_1}{\sqrt{2ah_0}}\right)\right); \end{aligned}$$

$$\begin{aligned} p(r)|_{r_1\le r\le r_2} = &-\int_r^{r_2}\frac{\partial p}{\partial r}(r)\bigg|_b dr - \int_{r_2}^{\infty}\frac{\partial p}{\partial r}(r)\bigg|_m dr = \\ &3Va\left[\eta_1 h^{-2}(r) + (\eta_0-\eta_1)h^{-2}(r_2)\right] + \\ &2\dot{\gamma}_c(\eta_0-\eta_1)\sqrt{\frac{2a}{h_0}}\times \\ &\left(\arctan\left(\frac{r_2}{\sqrt{2ah_0}}\right) - \arctan\left(\frac{r}{\sqrt{2ah_0}}\right)\right); \end{aligned}$$

$$p(r)|_{r>r_2} = -\int_{r_2}^{\infty}\frac{\partial p}{\partial r}(r)\bigg|_m dr = 3\eta_0 V a h^{-2}(r)$$

The force is therefore obtained simply by integration of the pressure along the tangential plane to the surface of the sphere

$$F = \int_0^\infty p(r)2\pi r dr = \begin{cases} F_1 & \text{if } h_0 \ge h_0^{lim} \\ \\ F_2 & \text{if } h_0 < h_0^{lim}. \end{cases} \tag{26}$$

Here, the quantity

$$h_0^{lim} = \frac{3}{4}\sqrt[3]{\frac{9}{2}\frac{V^2 a}{\dot{\gamma}_c^2}} \tag{27}$$

is calculated from the condition (16) and represents the minimum distance between spheres surfaces where the fluid has a mono-viscous Newtonian behavior, i.e. at smaller interparticle distances the fluid will be effectively bi-viscous. The expressions of F_1 and F_2 are given by

$$\begin{aligned} F_1 &= 6\pi\eta_0 V a^2 h_0^{-1} \\ F_2 &= 2\pi\left[3a^2\eta_0 V h_0^{-1} + 3a^2(\eta_0-\eta_1)V\left(h^{-1}(r_2)-h^{-1}(r_1)\right)\left(2-h_0\left(h^{-1}(r_1)+h^{-1}(r_2)\right)\right)+\right. \\ &\quad \left. 2a\dot{\gamma}_c(\eta_0-\eta_1)\left[(r_2-r_1)+(h(r_1)-2h_0)\sqrt{\frac{2a}{h_0}}\left(\arctan\left(\frac{r_2}{\sqrt{2ah_0}}\right)-\arctan\left(\frac{r_1}{\sqrt{2ah_0}}\right)\right)\right]\right] \end{aligned} \tag{28}$$

This is the central result of this work.

Clearly F_1 is exactly the same as the usual Newtonian normal force lubrication. More importantly, note that the correct Newtonian expression (F_1) is recovered from F_2 when we take $\eta_1 = \eta_0$, which represents a consistency check of the theory.

Moreover, in the limit $h_0 \to h_0^{lim}$, we have that $r_1 \to r_2$ (see Fig. 4) and the following expression holds

$$\lim_{h_0 \to h_0^{lim-}} F_2(h_0) = \lim_{h_0 \to h_0^{lim+}} F_1(h_0) \tag{29}$$

ensuring the continuity of the force as a function of h_0. In fact, the ratio h_0/h_0^{lim} gives us information about the importance of the bi-viscous behavior of the fluid, i.e. if $h_0/h_0^{lim} \geq 1$ the solvent behaves exactly as a Newtonian fluid with viscosity η_0, whereas if $h_0/h_0^{lim} \ll 1$, the solvent behaves essentially as a Newtonian fluid with viscosity η_1. The fluid has a transitional bi-viscous behavior between those two limits.

A. Calculation of r_1 and r_2

In order to use Eq. (28) to calculate the force acting between two spheres, we need to have an explicit expression for r_1 and r_2. Such a coordinates can be found by calculating the distances r where $\dot{\gamma}_s(r)$ is equal to $\dot{\gamma}_c$ (see Fig. 4), which leads us to the next equation

$$\left(\frac{r}{r_{max}}\right)^4 + 6\left(\frac{r}{r_{max}}\right)^2 - 16\left(\frac{\dot{\gamma}_s^{max}}{\dot{\gamma}_c}\right)\left(\frac{r}{r_{max}}\right) + 9 = 0 \tag{30}$$

where r_{max} was defined in (14). It is worth to note that the same expression can be obtained by doing $\frac{2z_c(r)}{h(r)} = 1$ in equation (19). Eq. (30) is a quartic equation which has unique real

solutions given by

$$r_1 = r_{max}\left[\mathcal{Q} - \sqrt{-3 - \mathcal{Q}^2 + 4\left(\frac{\dot{\gamma}_s^{max}}{\dot{\gamma}_c}\right)\frac{1}{\mathcal{Q}}}\right]$$
$$r_2 = r_{max}\left[\mathcal{Q} + \sqrt{-3 - \mathcal{Q}^2 + 4\left(\frac{\dot{\gamma}_s^{max}}{\dot{\gamma}_c}\right)\frac{1}{\mathcal{Q}}}\right] \tag{31}$$

where

$$\mathcal{Q} = \sqrt{-1 + \frac{1}{\mathcal{P}} + \mathcal{P}} \tag{32}$$
$$\mathcal{P} = \sqrt[3]{-1 + 2\left(\frac{\dot{\gamma}_s^{max}}{\dot{\gamma}_c}\right)^2 + 2\left(\frac{\dot{\gamma}_s^{max}}{\dot{\gamma}_c}\right)\sqrt{\left(\frac{\dot{\gamma}_s^{max}}{\dot{\gamma}_c}\right)^2 - 1}}$$

B. Limiting behaviors

With the full lubrication solution obtained, i.e. Eqs. (28) and (31), we can calculate now several interesting limits. First, if we take the limit $\dot{\gamma}_c \to 0$, we have that $r_1 \to 0$, $r_2 \to \infty$ and $h_0^{lim} \to \infty$ so the force reduces trivially to the case of a Newtonian fluid of viscosity η_1.

Another interesting limit is obtained when the spheres are almost touching $h_0 \to 0$. In this case, by using Eqs. (14) and (15), the quartic expression (30) can be written as

$$\frac{1}{4a^2h_0^2}r^4 + \frac{1}{ah_0}r^2 - \frac{3V}{\dot{\gamma}_c h_0^2}r + 1 = 0 \tag{33}$$

In the limit $h_0 \to 0$ only the first and third terms are relevant, so the equation to solve simplifies to

$$\frac{1}{4a^2h_0^2}r^4 - \frac{3V}{\dot{\gamma}_c h_0^2}r = 0 \tag{34}$$

whose solutions provide us the limits of r_1 and r_2 for $h_0 \to 0$, which are

$$\lim_{h_0\to 0} r_1 = 0$$
$$r_2^{lim} \equiv \lim_{h_0\to 0} r_2 = \sqrt[3]{\frac{12Va^2}{\dot{\gamma}_c}} \tag{35}$$

In this limit the force (28) reduces to the one of a Newtonian fluid with viscosity η_1

$$\lim_{h_0\to 0} F\Big|_{\eta_1\neq 0} = 6\pi\eta_1 V a^2 h_0^{-1} \tag{36}$$

where we assume that $\eta_1 \neq 0$.

Let us consider now the case where we take $\eta_1 = 0$ in the equations, i.e. we have a bi-viscous fluid characterized by a zero-resistance above a certain critical shear-rate. In this case the force in the limit $h_0 \to 0$ reads as

$$F_{max} \equiv \lim_{h_0 \to 0} F \Big|_{\eta_1 = 0} = 6\pi\eta_0 V a^2 d_0^{-1} \tag{37}$$

where

$$d_0 = \frac{2}{9}\sqrt[3]{4}\; h_0^{lim} \approx 0.35 h_0^{lim} \tag{38}$$

Note that F_{max} does not depend on the gap h_0 between the surfaces of the spheres, imposing a finite limit in the lubrication force when $\eta_1/\eta_0 \to 0$. This is due to the fact that, for $h_0 \to 0$, all the lubrication force comes from the friction between the surface of the sphere and the solvent in the region $r > r_2^{lim}$. Note that r_2^{lim} is not an artifact of the lubrication approximation because, given a certain physical $\dot{\gamma}_c$ and a, we can always choose a relative velocity V sufficiently small such that $r_2^{lim} \ll a$ is within the lubrication regime. It is worth mentioning that in the limit $\eta_1 \to 0$ the local Reynolds number in the boundary layer of vanishing viscosity remains finite, in such a way that the lubrication assumptions can still be valid. (see Appendix B).

IV. MODEL PREDICTIONS

In this section we apply the model to do predictions about the lubrication force between spherical particles immersed in a liquid with rheology characterized by a bi-viscous behavior. This is a good model for a variety of complex fluids characterized by approximate constant viscosity up to a given shear rates $\dot{\gamma}_c$, followed by a significant shear-thinning. Examples include many polymeric fluids[44–47]. Specifically we are going to focus on polydimethylsiloxane (PDSM) liquids. Given their long range of shear rates where the fluid behaves as Newtonian ($> 1000\ s^{-1}$) and their relatively high zero-shear viscosity[40–42], they have been widely used as a Newtonian solvent in rheological studies of suspensions[48–51].

As a prototype system, we explore the particle lubrication interaction between two equal spheres of radius $R = 50\ \mu m$, which is a typical size for a non-colloidal particle in suspension. Note that the real radius $R = 2a$, where a is the reduced radius defined in Sec. III. The spheres are approaching each other along the line joining their centers of mass at a relative

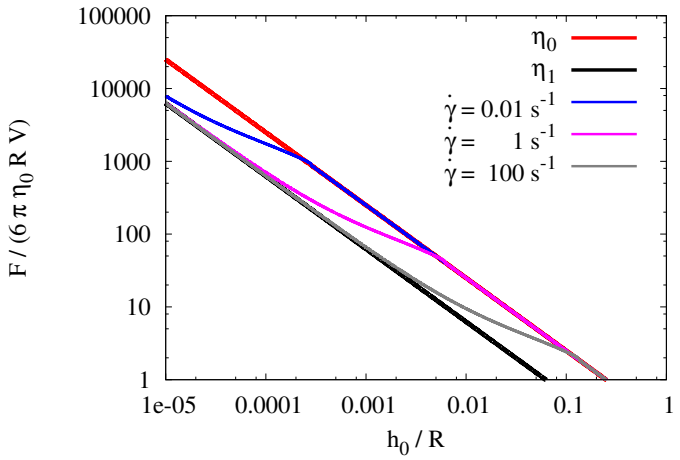

FIG. 5. Force of lubrication for different $\dot{\gamma}$ of two equal spheres of radius $R = 50\ \mu m$ in a bi-viscous fluid with $\eta_1/\eta_0 = 0.25$ and $\dot{\gamma}_c = 1000\ s^{-1}$.

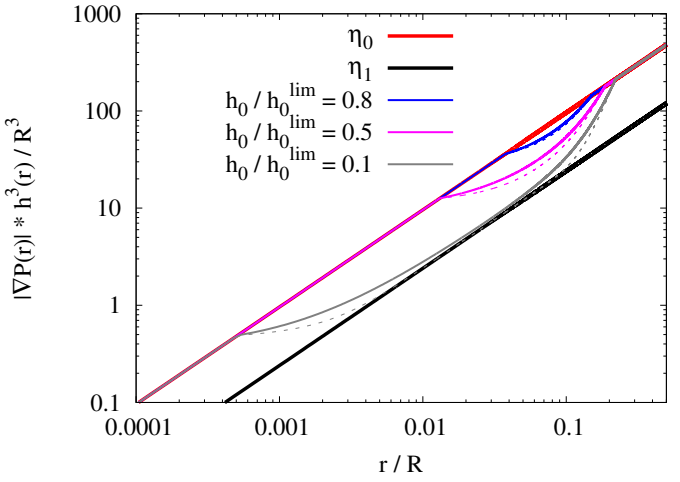

FIG. 6. Comparison of the approximated pressure gradient $\nabla P(r) = \partial p/\partial r(r)$ (solid line) with the exact solution (dashed line) at different distances between spheres, for the case $\eta_1/\eta_0 = 0.25$, $\dot{\gamma}_c = 1000\ s^{-1}$, $\dot{\gamma} = 1\ s^{-1}$.

velocity $V = a\dot{\gamma}$. $\dot{\gamma}$ is the average shear rate around the particle and we will consider that is ranged between $10^{-2}\ s^{-1}$ and $10^{2}\ s^{-1}$ which are values typical probed in experiments using standard rheometers.

A. Effect of shear rate $\dot{\gamma}$

We start studying the effect of the shear rate $\dot{\gamma}$ on the interparticle lubrication force by changing the relative velocity V. Fluid parameters have been chosen to match a standard PDMS-liquid, i.e. viscosity ratio $\eta_1/\eta_0 = 0.25$ and $\dot{\gamma}_c = 1000\ s^{-1}$. In Fig. 5 we have drawn the results for three different regimes $\dot{\gamma} = 0.01,\ 1,\ 100\ s^{-1}$. For this set of physical parameters, at the lowest shear rate the fluid behaves essentially as a Newtonian with viscosity η_0 (blue-red lines, Fig. 5) in the physically interesting regime. Note that at interparticle distances $h_0 < 10^{-4}R$ the smooth-surface approximation becomes questionable as roughness typically exceeds this value, even for large non-colloidal particles. Note however that high-precision fabrication of microspheres with surface roughness $< 1\ nm$ is already possible[52].

In the opposite limit, i.e. at the highest shear rate, the lubrication force is consistent with that of a Newtonian fluid with viscosity η_1 (gray-black lines, Fig. 5) in the lubrication regime, i.e. for $h_0/a \ll 1$. A continuous transition between the two solutions is finally observed for $\dot{\gamma} = 1\ s^{-1}$ (pink line), where the truly bi-viscous nature of the problem becomes relevant in the lubrication regime.

This result shows also that, under the prescribed physical conditions, shear-thinning effects in the lubrication force (transition) can practically take place for a non-colloidal particle system in a range of macroscopic $\dot{\gamma} \in [0.01 : 100]\ s^{-1}$. This could represent a possible mechanism to explain the puzzling shear-thinning behavior often observed in non-colloidal systems[48–51].

In order to check the accuracy of the model respect to the exact analytical solution, we have drawn in the Fig. 6 the comparison between the approximation to $\frac{\partial p}{\partial r}(r)$ obtained by Eq. (24) with the exact solution calculated from Eqs. (20) and (8) for the previous case with $\dot{\gamma} = 1\ s^{-1}$, at different distances. The agreement is overall very good. This can be viewed also as 'a posteriori' justification of the main assumption made in Eq. (22). A more detailed analysis of the error on the force is presented in Appendix A.

B. Effect of η_1/η_0 and $\dot{\gamma}_c$

By modifying the length and polydispersity of the PDMS molecules, for example, one can practically change the rheological properties of a PDMS-liquid, such as the range of shear

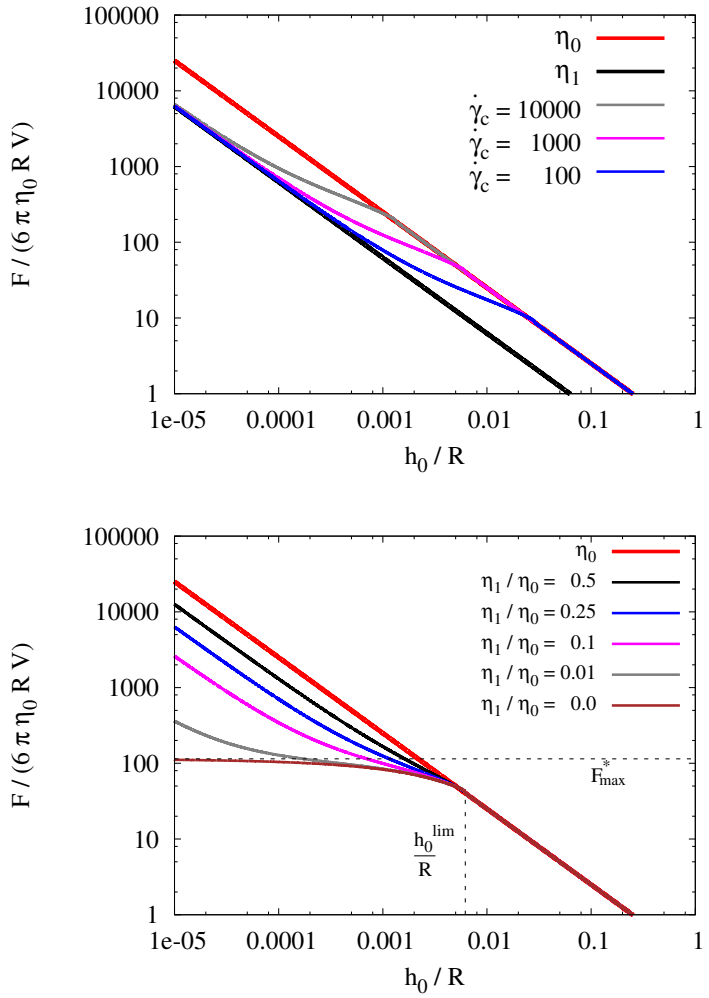

FIG. 7. Lubrication force between two equal spheres of radius $R = 50\ \mu m$ in different fluids with a shear rate $\dot{\gamma} = 1\ s^{-1}$. In the first one, the ratio $\eta_1/\eta_0 = 0.25$ remains fixed, and the effect of changing the parameter $\dot{\gamma}_c$ is studied. In the second one the shear rate $\dot{\gamma} = 1\ s^{-1}$ while the ratio η_1/η_0 is changed. Distance h_0 and force $F^*_{max} \equiv F_{max}/(6\pi\eta_0 RV)$ given by eqs. (38) and (37) have been also drawn as reference.

rates where it behaves as (close to) Newtonian or the onset of power-law viscosity regime[41]. Such changes can be taken into account in our model by tuning the viscosity ratio η_1/η_0 and the cutoff shear rate $\dot{\gamma}_c$. In the following, we study the effects of changing these parameters.

In the first graph of Fig. 7 we can see the effect of changing $\dot{\gamma}_c$ between 100 s^{-1} and 10000 s^{-1} in a fluid with $\eta_1/\eta_0 = 0.25$ undergoing an average $\dot{\gamma} = 1\ s^{-1}$. We can observe that by increasing $\dot{\gamma}_c$ the transitional behavior (where the bi-viscous nature of the fluid

rheology is relevant) is moved towards smaller interparticle distances.

In the second graph of the same figure we have changed the ratio η_1/η_0 in the range 0 to 0.5 in a fluid with $\dot{\gamma}_c = 1000\ s^{-1}$ and $\dot{\gamma} = 1\ s^{-1}$. This change affects the slope of the lubrication force at short ranges, but does not influence the critical distance h_0^{lim} for its onset, which does not depend on η_1/η_0 (see Eq. (27)). When $\eta_1/\eta_0 \to 1$ the fluid is approaching the Newtonian case with viscosity η_0, as calculated already before. Note that the range where the transition between viscosities η_0 and η_1 takes place, increases for smaller ratios η_1/η_0, until it reaches a limit, where the lubrication force F_{max} is nearly constant for $\eta_1/\eta_0 \to 0$.

Note that this limiting expression for the force can be interpreted as a possible solvent-mediated regularization mechanism for the unrealistic diverging behavior of lubrication at vanishing interparticle gap. This is typically explained based on the fact that the Stokes approximation fails at small distances where either surface roughness or non-hydrodynamic surface-surface interactions (i.e. electrostatic) occur. The present results show also that this can happen when the fluid does not longer behave as a constant-viscosity Newtonian. As most of simple fluids under extremely large shear rates eventually show significant shear-thinning[17], this interpretation offers a formal way to introduce a cutoff in the singular resistance based on suspending medium rheology.

C. Low-viscosity regions

In this section we study in detail the local topology of the interface separating fluid regions with viscosity η_1, in the following termed *low-viscosity regions*, from those where the viscosity is η_0 (*high-viscosity regions*). In particular we show how these regions change in the gap between spheres for different model parameters. As done before, we consider the squeezing flow between two equal spheres of radius $R = 50\ \mu m$ in relative approaching motion.

We start keeping fixed the following parameters: $\eta_1/\eta_0 = 0.25$, $h_0 = 4 \times 10^{-3} R$ and $\dot{\gamma} = 1\ s^{-1}$, and consider uniquely the change of $\dot{\gamma}_c$ in the range $100 - 500\ s^{-1}$. When the value of $\dot{\gamma}_c$ is increased, the distance $r_2 - r_1$ is reduced (see Fig. 4). Simultaneously, the low-viscosity regions are located in a vanishing area close to the sphere's walls, i.e. between r_1 and r_2 where the local shear rates are higher (see Fig. 8 where low-viscosity regions are

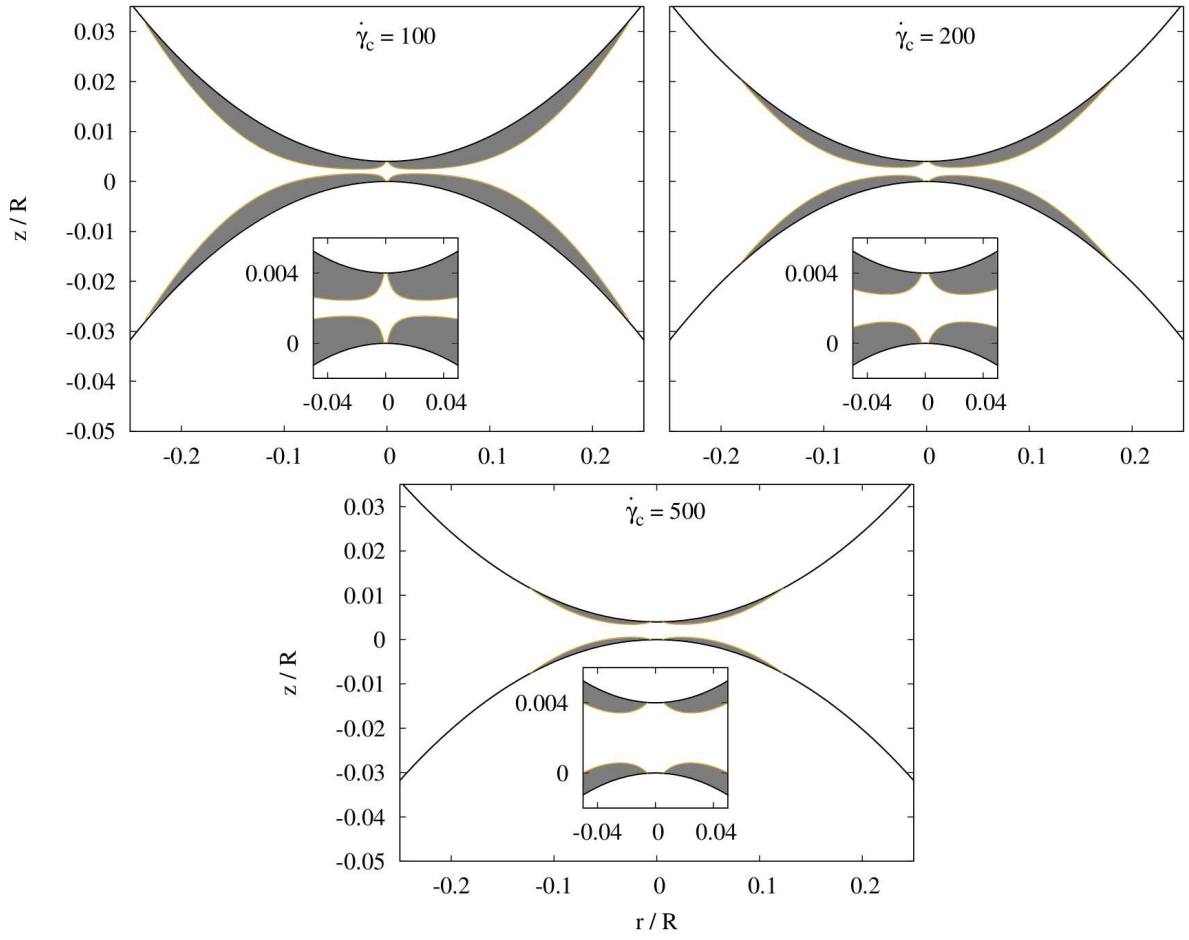

FIG. 8. Low-viscosity regions for the squeezing flow between two equal spheres of radius $R = 50\ \mu m$ separated by a gap $h_0 = 4 \times 10^{-3} R$ in a fluid with $\dot{\gamma} = 1\ s^{-1}$ and $\eta_1/\eta_0 = 0.25$, where $\dot{\gamma}_c$ is changed in the range $100 - 500\ s^{-1}$.

depicted as shadowed areas). In the limit $\dot{\gamma}_c \to \dot{\gamma}_s^{max}$, $r_1 = r_2$ and the low-viscosity regions will disappear, recovering the behavior of a Newtonian fluid of viscosity η_0.

On opposite, in the limit $\dot{\gamma}_c \to 0$, r_1 tends to 0 and r_2 to infinity, in such a way that the low viscosity regions would occupate the whole space, recovering the behavior of a Newtonian fluid of viscosity η_1. In the insets of Fig. 8 the central region of the channel between the particles has been drawn. There will always be a high viscosity region in the center due to the fact that the shear rate tends to zero when approaching $r = 0$.

In Fig. 9 we fix the parameters: $\dot{\gamma}_c = 100\ s^{-1}$, $h_0 = 4 \times 10^{-3} R$ and $\dot{\gamma} = 1\ s^{-1}$ and change the ratio η_1/η_0 in the range $0.02 - 0.5$. In this case, given that r_1 and r_2 do not depend on η_1/η_0, they remain fixed for the three cases shown in the figure. In fact, as long as the

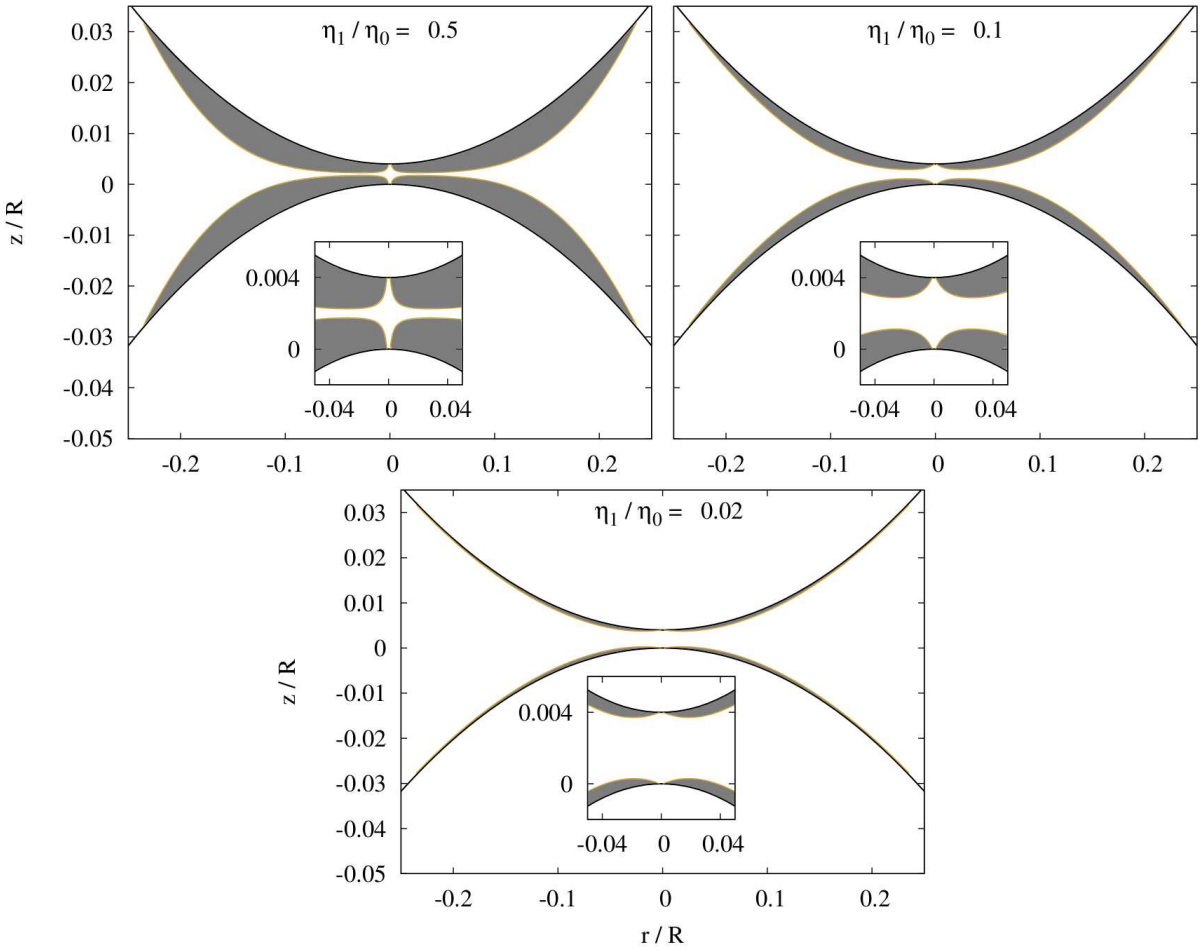

FIG. 9. Low-viscosity regions for the squeezing flow between two equal spheres of radius $R = 50\ \mu m$ separated by a gap $h_0 = 4 \times 10^{-3} R$ in a fluid with $\dot{\gamma} = 1\ s^{-1}$ and $\dot{\gamma}_c = 100\ s^{-1}$, where $\eta_1/\eta_0 = 0.25$ is changed in the range $0.02 - 0.5$.

condition (16) is held, there will be, for any ratio η_1/η_0, a low-viscosity region between the coordinates r_1 and r_2. As η_1/η_0 is increased, the low viscosity region will be wider, reaching, in the limit $\eta_1/\eta_0 \to 1$, an extension whose topology can be calculated from the limit of eq. (23) as

$$\lim_{\eta_1/\eta_0 \to 1} z_c(r) = \frac{h(r)}{2} \frac{\dot{\gamma}_c}{\dot{\gamma}_s(r)} \tag{39}$$

Note that such a region is wider when $\dot{\gamma}_c$ is increased, but will never occupy the whole space between r_1 and r_2, i.e. $z_c \to h(r)/2$ for all r, given that, $\dot{\gamma}_c \leq \dot{\gamma}_s^{max}$ in the coordinates $r_1 < r < r_2$. In such a limit, independently on the topology described above, the case of a fluid of viscosity η_0 is recovered because the two viscosities are the same. In the insets

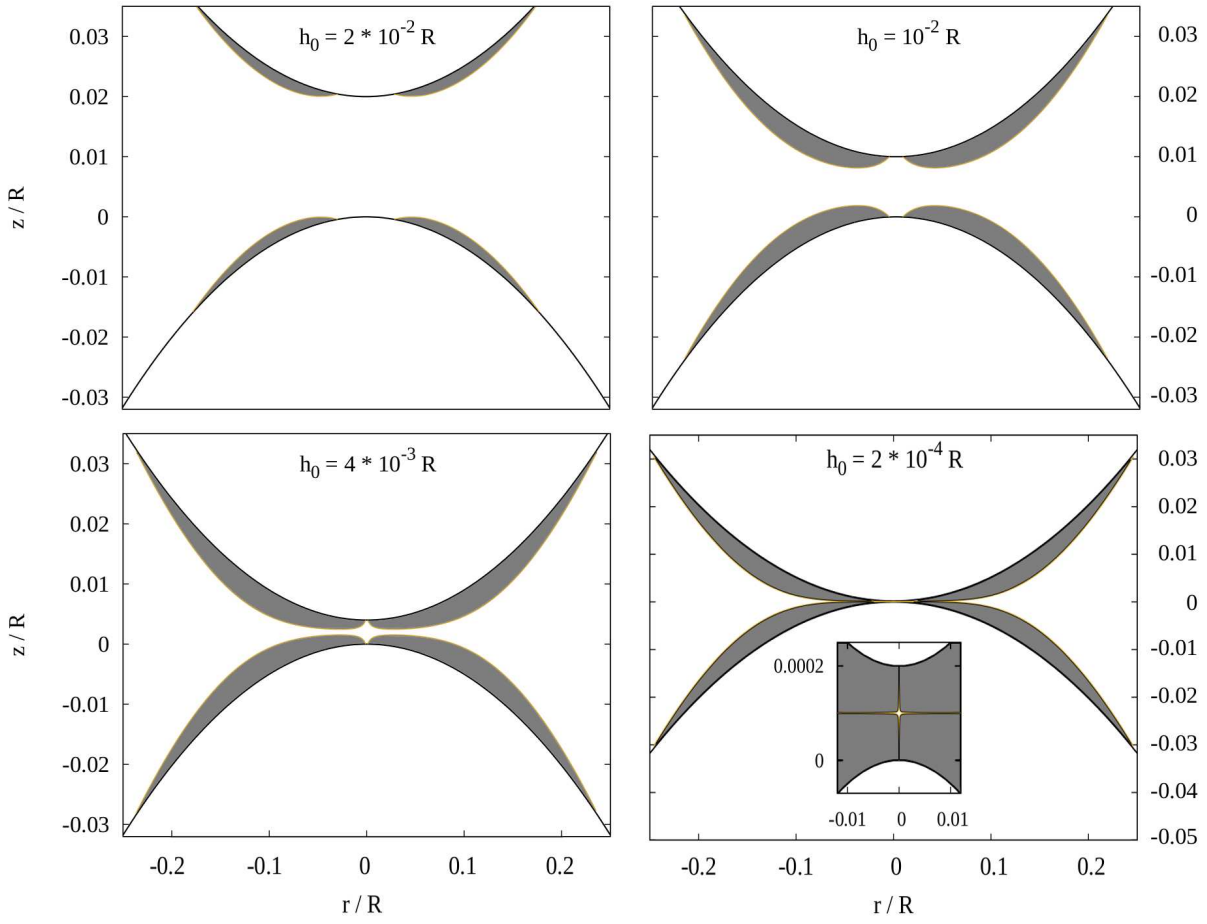

FIG. 10. Low-viscosity regions for the squeezing flow between two equal spheres of radius $R = 50\ \mu m$ in a fluid with $\dot{\gamma} = 1\ s^{-1}$ and $\dot{\gamma}_c = 100\ s^{-1}$, and $\eta_1/\eta_0 = 0.25$ where the gap h_0 is changed in the range $2 \times 10^{-2}R - 2 \times 10^{-4}R$.

of Fig. 9 it can better appreciated how, although the width of the low viscosity region is decreasing when η_1/η_0 becomes smaller, the value of r_1 remains the same.

On opposite, when η_1/η_0 is decreased, the low viscosity region will become increasingly thinner. The limit $\eta_1/\eta_0 \to 0$ defines a boundary layer located between r_1 and r_2 which will not contribute whatsoever to the lubrication force. In this limit the only contribution to such a force comes from the friction within the fluid at radial distances $r < r_1$ and $r > r_2$. Note that, in this case of vanishing η_1, if the gap is decreased to the *almost touching* limit, given that $r_1 \to 0$, only the outer region of the gap, i.e, $r > r_2$, will contribute to the friction.

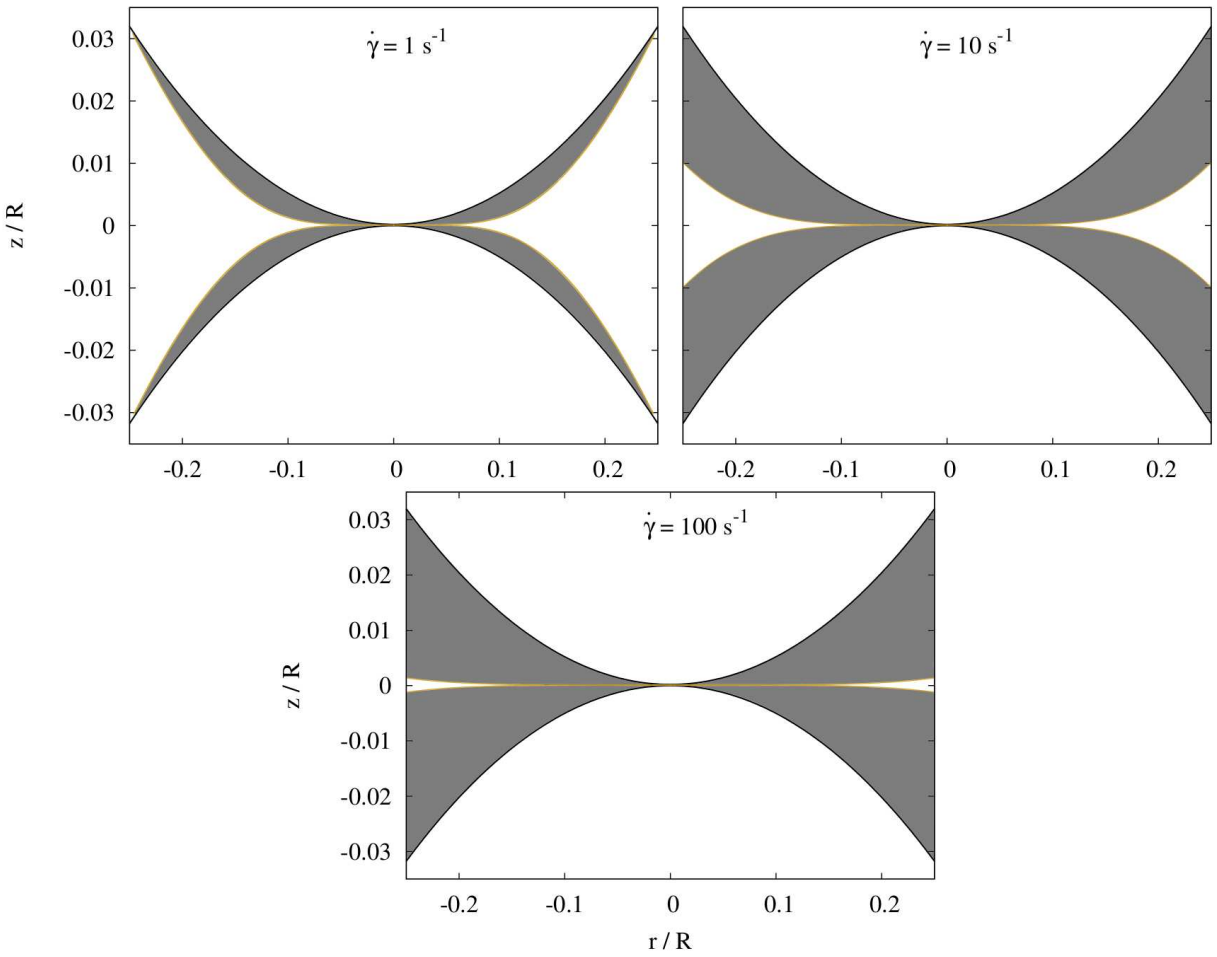

FIG. 11. Low-viscosity regions for the squeezing flow between two equal spheres of radius $R = 50\ \mu m$ almost on contact ($h_0 = 2 \times 10^{-4} R$) in a fluid with $\dot{\gamma}_c = 100\ s^{-1}$, and $\eta_1/\eta_0 = 0.25$ where $\dot{\gamma}$ is changed in the range $1 - 100$.

As a further test, we consider the case where we keep fixed the parameters of the fluid to $\dot{\gamma}_c = 100\ s^{-1}$, $\eta_1/\eta_0 = 0.25$ and $\dot{\gamma} = 1\ s^{-1}$, and change uniquely the gap between spheres in the range $h_0 = 2 \times 10^{-2} R - 2 \times 10^{-4} R$ (see Fig. 10). When the two spheres get closer, r_1 and r_2 tend to their limits, i.e. 0 and r_2^{lim} given by Eq. (35), and the low-viscosity regions become wider, spreading into the bulk and reaching a maximum extension in the limit $h_0 \to 0$. This can be calculated from the limit of z_c, given by Eq. (23), as

$$\lim_{h_0 \to 0} z_c(r) = \frac{r^2}{4a} \frac{\eta_0}{\eta_0 - \eta_1 \left(1 - \left(\frac{r_2^{lim}}{r}\right)^3\right)} \tag{40}$$

As a result, the low-viscosity regions in Fig. 10 in the case where the particles are closer are

indistinguishable from the ones in the limit $h_0 \to 0$. Note that $r^2/(4a)$ is half the gap at r, so the low viscosity region will occupy the whole gap only if $\eta_1 = 0$. In the inset of Fig. 10 it can be appreciated how the central region of the channel is substantially characterized by low viscosity, except for the very narrow regions around $r = 0$ and $z = c(r)$.

If in such a limit of vanishing h_0, the relative velocity is increased, as it is shown in Fig. 11 (where we have changed $\dot{\gamma}$ in the range $1 - 100\ s^{-1}$), the low viscosity regions will eventually grow. In the limit of large relative velocities ($\dot{\gamma} \gg 1$) the whole gap between the spheres will be occupied by a low-viscosity region and, again, the case of a Newtonian fluid with viscosity η_1 is recovered.

V. CONCLUSION

In this article we have presented an analytical solution for the lubrication force between two spheres moving in a bi-viscous fluid characterized by a low shear rate viscosity η_0 and a high shear rate viscosity η_1. The obtained lubrication force shows a cross-over between the known expressions in the two limiting Newtonian cases, i.e. (i) it reduces consistently to the case of a simple Newtonian fluid with viscosity η_0 when $\dot{\gamma}_c \gg \dot{\gamma}$ and (ii) it reduces to the case of a Newtonian fluid with viscosity η_1 when $\dot{\gamma}_c \ll \dot{\gamma}$. In the limit of equal viscosities, the standard lubrication formula is recovered.

An interesting result of the theory is that in the limit of vanishing viscosity ratio, i.e. $\eta_1/\eta_0 \to 0$, the lubrication force is not longer singular for a vanishing gap between spheres. Technically, this is due to the fact that in this limit, a boundary layer of very low-viscosity is formed along the spheres surfaces in their closest region, which will not contribute to the overall dissipation. Lubrication contribution comes therefore only from regions placed radially apart from the near-contact area, which are not longer influenced by the infinitesimal change in the gap. The present result offers a formal way to regularize the singular resistance due to lubrication based on non-Newtonian suspending medium rheology.

It should be remarked that the current model could be also used to study effect of viscoplastic suspending media characterized by apparent yield stress whith two finite viscosity-plateaus[53].

The new model for inter-particle lubrication forces presented here can also pave the ways for novel effective lubrication-dynamics simulations to study the flow and rheology of

complex particulate systems in the future[18].

ACKNOWLEDGMENTS

The Authors gratefully acknowledge the financial support provided by the Welsh Government and Higher Education Funding Council for Wales through the Ser Cymru National Research Network in Advanced Engineering and Materials. Computing resources offered by HPC Wales via the project Nr. HPCWT050 (Multiscale particle simulation for complex fluids) is also gratefully acknowledged.

REFERENCES

[1]R. I. Tanner, *Engineering rheology*, 2nd ed. (Oxford University Press New York, 2000) p. p. cm.

[2]J. Mewis and N. J. Wagner, *Colloidal Suspension Rheology* (Cambridge University Press, 2011).

[3]A. Einstein, *Investigations on the Theory of the Brownian Movement* (Courier Corporation, 1956).

[4]G. Batchelor, "The stress system in a suspension of force-free particles," Journal of fluid mechanics **41**, 545–570 (1970).

[5]G. Batchelor and J. Green, "The determination of the bulk stress in a suspension of spherical particles to order c2," Journal of Fluid Mechanics **56**, 401–427 (1972).

[6]G. Batchelor, "The effect of brownian motion on the bulk stress in a suspension of spherical particles," Journal of Fluid Mechanics **83**, 97–117 (1977).

[7]J. J. Stickel and R. L. Powell, "Fluid mechanics and rheology of dense suspensions," Annu. Rev. Fluid Mech. **37**, 129–149 (2005).

[8]R. I. Tanner, "Non-colloidal suspensions: Relations between theory and experiment in shearing flows," Journal of Non-Newtonian Fluid Mechanics **222**, 18 – 23 (2015).

[9]W. R. Hwang, M. A. Hulsen, and H. E. Meijer, "Direct simulation of particle suspensions in sliding bi-periodic frames," Journal of Computational Physics **194**, 742 – 772 (2004).

[10]G. D'Avino, P. Maffettone, M. Hulsen, and G. Peters, "A numerical method for simulating

concentrated rigid particle suspensions in an elongational flow using a fixed grid," Journal of Computational Physics **226**, 688 – 711 (2007).

[11]A. Ladd and R. Verberg, "Lattice-boltzmann simulations of particle-fluid suspensions," Journal of Statistical Physics **104**, 1191–1251 (2001).

[12]N. S. Martys, "Study of a dissipative particle dynamics based approach for modeling suspensions," Journal of Rheology **49**, 401–424 (2005).

[13]A. Sierou and J. F. Brady, "Accelerated stokesian dynamics simulations," Journal of Fluid Mechanics **448**, 115–146 (2001).

[14]X. Bian and M. Ellero, "A splitting integration scheme for the sph simulation of concentrated particle suspensions," Computer Physics Communications **185**, 53–62 (2014).

[15]A. Vázquez-Quesada, X. Bian, and M. Ellero, "Three-dimensional simulations of dilute and concentrated suspensions using smoothed particle hydrodynamics," Computational Particle Mechanics **1**, 36 (2015).

[16]A. Vázquez-Quesada and M. Ellero, "Rheology and microstructure of non-colloidal suspensions under shear studied with smoothed particle hydrodynamics," Journal of Non-Newtonian Fluid Mechanics (2016).

[17]S. Hess, C. Aust, L. Bennett, M. Kröger, C. P. Borgmeyer, and T. Weider, "Rheology: From simple and to complex fluids," Physica A: Statistical Mechanics and its Applications **240**, 126–144 (1997).

[18]G. Ovarlez, F. Mahaut, S. Deboeuf, N. Lenoir, S. Hormozi, and X. Chateau, "Flows of suspensions of particles in yield stress fluids," Journal of Rheology **59**, 1449–1486 (2015).

[19]H. Brenner and J. Happel, "Low reynolds number hydrodynamics," (1965).

[20]M. Cooley and M. O'neill, "On the slow motion of two spheres in contact along their line of centres through a viscous fluid," in *Mathematical Proceedings of the Cambridge Philosophical Society*, Vol. 66 (Cambridge Univ Press, 1969) pp. 407–415.

[21]M. E. O'Neill and S. R. Majumdar, "Asymmetrical slow viscous fluid motions caused by the translation or rotation of two spheres. part ii: Asymptotic forms of the solutions when the minimum clearance between the spheres approaches zero," Zeitschrift für angewandte Mathematik und Physik ZAMP **21**, 180–187 (1970).

[22]P. Ganatos, R. Pfeffer, and S. Weinbaum, "A numerical-solution technique for three-dimensional stokes flows, with application to the motion of strongly interacting spheres in a plane," Journal of Fluid Mechanics **84**, 79–111 (1978).

[23]D. Jeffrey, "Low-reynolds-number flow between converging spheres," Mathematika **29**, 58–66 (1982).

[24]D. Jeffrey and Y. Onishi, "Calculation of the resistance and mobility functions for two unequal rigid spheres in low-reynolds-number flow," Journal of Fluid Mechanics **139**, 261–290 (1984).

[25]D. Jeffrey and Y. Onishi, "The forces and couples acting on two nearly touching spheres in low-reynolds-number flow," Zeitschrift für angewandte Mathematik und Physik ZAMP **35**, 634–641 (1984).

[26]D. Jeffrey and R. Corless, "Forces and stresslets for the axisymmetric motion of nearly touching unequal spheres," PhysicoChemHydrodyn **10**, 461 (1988).

[27]S. Kim and S. Karrila, "Microhydrodynamics: Principles and applications," (1991).

[28]D. Jeffrey, "The calculation of the low reynolds number resistance functions for two unequal spheres," Physics of Fluids A: Fluid Dynamics **4**, 16–29 (1992).

[29]G. J. Rodin, "Squeeze film between two spheres in a power-law fluid," Journal of non-newtonian fluid mechanics **63**, 141–152 (1996).

[30]G. Lian, Y. Xu, W. Huang, and M. J. Adams, "On the squeeze flow of a power-law fluid between rigid spheres," Journal of Non-Newtonian Fluid Mechanics **100**, 151–164 (2001).

[31]W. Huang, H. Li, Y. Xu, and G. Lian, "Hydrodynamic force between two hard spheres tangentially translating in a power-law fluid," Chemical engineering science **61**, 1480–1488 (2006).

[32]C. Xu, L. Yuan, Y. Xu, and W. Hang, "Squeeze flow of interstitial herschel–bulkley fluid between two rigid spheres," Particuology **8**, 360–364 (2010).

[33]H. Wen-bin, X. Yong, L. Guo-ping, and L. Hong-yan, "Squeeze flow of a power-law fluid between two rigid spheres with wall slip," Applied Mathematics and Mechanics **23**, 811–818 (2002).

[34]H. Li, W. Huang, Y. Xu, and G. Lian, "On the squeeze flow of a bingham fluid between two rigid spheres," Particulate Science and Technology , 1–20 (2004).

[35]R. I. Tanner and J. F. Milthorpe, "Numerical simulation of the flow of fluids with yield stresses," in *In Proceeding of the International Conference on 'Numerical Methods in Laminar and Turbulent Flow'* (1983) pp. 680–690.

[36]D. K. Gartling and N. Phan-Thien, "A numerical simulation of a plastic fluid in a parallel-plate plastometer," Journal of non-Newtonian fluid mechanics **14**, 347–360 (1984).

[37]E. Mitsoulis, "Flows of viscoplastic materials: models and computations," in *In Rheology Reviews 2007. British Society of Rheology* (2007).

[38]N. J. Balmforth, I. A. Frigaard, and G. Ovarlez, "Yielding to stress: Recent developments in viscoplastic fluid mechanics," Annual Review of Fluid Mechanics **46**, 121–146 (2014).

[39]G. Ovarlez, S. Cohen-Addad, K. Krishan, J. Goyon, and P. Coussot, "On the existence of a simple yield stress fluid behavior," Journal of Non-Newtonian Fluid Mechanics **193**, 68–79 (2013).

[40]T. Kataoka and S. Ueda, "Flow behavior of polydimethylsiloxane," Journal of Polymer Science Part A: General Papers **3**, 2947–2954 (1965).

[41]C. Lee, K. Polmanteer, and E. King, "Flow behavior of narrow-distribution polydimethylsiloxane," Journal of Polymer Science Part A-2: Polymer Physics **8**, 1909–1916 (1970).

[42]F. E. Swallow, "Viscosity of polydimethylsiloxane gum: shear and temperature dependence from dynamic and capillary rheometry," Journal of applied polymer science **84**, 2533–2540 (2002).

[43]E. Guazzelli and J. F. Morris, *A physical introduction to suspension dynamics* (Cambridge University Press, 2011).

[44]D. V. Boger, "Demonstration of upper and lower newtonian fluid behaviour in a pseudoplastic fluid," Nature **265**, 126–128 (1977).

[45]R. B. Bird, R. C. Armstrong, O. Hassager, and C. F. Curtiss, *Dynamics of polymeric liquids*, Vol. 1 (Wiley New York, 1977).

[46]R. Chhabra and P. Uhlherr, "Estimation of zero-shear viscosity of polymer solutions from falling sphere data," Rheologica acta **18**, 593–599 (1979).

[47]Z. Zhang and G. F. Christopher, "The nonlinear viscoelasticity of hyaluronic acid and its role in joint lubrication," Soft matter **11**, 2596–2603 (2015).

[48]F. Ferrini, D. Ercolani, B. de Cindio, L. Nicodemo, L. Nicolais, and S. Ranaudo, "Shear viscosity of settling suspensions," Rheologica Acta **18**, 289–296 (1979).

[49]F. Gadala-Maria and A. Acrivos, "Shear-induced structure in a concentrated suspension of solid spheres," Journal of Rheology **24**, 799–814 (1980).

[50]S.-C. Dai, E. Bertevas, F. Qi, and R. I. Tanner, "Viscometric functions for noncolloidal sphere suspensions with newtonian matrices," Journal of Rheology **57**, 493–510 (2013).

[51]R. I. Tanner, "Non-colloidal suspensions: Relations between theory and experiment in shearing flows," Journal of Non-Newtonian Fluid Mechanics (2014).

[52]M.-C. M. Lee and M. C. Wu, "Thermal annealing in hydrogen for 3-d profile transformation on silicon-on-insulator and sidewall roughness reduction," Journal of Microelectromechanical systems **15** (2006).

[53]H. A. Barnes, "The yield stress –a review or $\pi\alpha\nu\tau\alpha$ $\rho\varepsilon\iota$– everything flows?" Journal of Non-Newtonian Fluid Mechanics **81**, 133–178 (1999).

Appendix A: Model error analysis

In this appendix we check the accuracy of the model by comparing it to the exact analytical solution. First, we demonstrate that the error in the calculated lubrication force can be expressed by only two variables. Secondly, we compare numerically the model to the exact analytical solution.

In order to simplify the calculations, the following dimensionless quantities are introduced

$$\overline{\eta} = \frac{\eta_1}{\eta_0}, \qquad \overline{r} = \frac{r}{r_{max}}, \qquad \overline{h} = \frac{h_0}{h_0^{lim}} \tag{A1}$$

Note that the present model requires $0 \leq \overline{\eta} \leq 1$. Its bi-viscous behavior is present only at the regions $\overline{r}_1 < \overline{r} < \overline{r}_2$ (where $\overline{r}_{1,2} = r_{1,2}/r_{max}$) and $0 \leq \overline{h} < 1$. Let us also define the quantity $\overline{\dot{\gamma}}(r) = \dot{\gamma}_s(r)/\dot{\gamma}_c$ which can be rewritten in term of the above variables (A1) as

$$\overline{\dot{\gamma}}\left(\overline{r},\overline{h}\right) = \frac{16}{9}\overline{r}\left[\overline{h}^{3/2}\left(1+\frac{1}{3}\overline{r}^2\right)^2\right]^{-1} \tag{A2}$$

Let us consider also the following dimensionless variable $\overline{z}_c$ defined as

$$\begin{aligned}
\overline{z}_c\left(\overline{\eta},\overline{r},\overline{h}\right)\Big|^{\text{exact}} &= \frac{2z_c}{h}\left(\overline{\eta},\overline{r},\overline{h}\right)\Big|^{\text{exact}} = S_1\left(\overline{\eta},\overline{r},\overline{h}\right) + S_2\left(\overline{\eta},\overline{r},\overline{h}\right) \\
\overline{z}_c\left(\overline{\eta},\overline{r},\overline{h}\right)\Big|^{\text{approx}} &= \frac{2z_c}{h}\left(\overline{\eta},\overline{r},\overline{h}\right)\Big|^{\text{approx}} = \frac{1}{1-\overline{\eta}\left(1-\overline{\dot{\gamma}}\left(\overline{r},\overline{h}\right)\right)}
\end{aligned} \tag{A3}$$

where

$$\begin{aligned}
S_1(r) &= \sqrt[3]{\frac{1}{2(1-\overline{\eta})}\left(1+\sqrt{1+\frac{4}{27}\frac{\overline{\eta}^3}{1-\overline{\eta}}\overline{\dot{\gamma}}\left(\overline{r},\overline{h}\right)^3}\right)} \\
S_2(r) &= \sqrt[3]{\frac{1}{2(1-\overline{\eta})}\left(1-\sqrt{1+\frac{4}{27}\frac{\overline{\eta}^3}{1-\overline{\eta}}\overline{\dot{\gamma}}\left(\overline{r},\overline{h}\right)^3}\right)}
\end{aligned} \tag{A4}$$

The pressure gradient can be written as

$$\begin{aligned}\left.\frac{\partial p}{\partial r}(r)\right|_b^{\text{approx, exact}} &= -C\ f_b\left(\overline{\eta},\overline{r},\overline{h}\right)\Big|^{\text{approx,exact}}\\ \left.\frac{\partial p}{\partial r}(r)\right|_m &= -C\ f_m\left(\overline{r},\overline{h}\right)\end{aligned} \tag{A5}$$

where $C = 2\dot{\gamma}_c\eta_0/h_0$ and

$$\begin{aligned}f_b\left(\overline{\eta},\overline{r},\overline{h}\right)\Big|^{\text{approx,exact}} &= \frac{\overline{z}_c^{-1}\left(\overline{\eta},\overline{r},\overline{h}\right)\Big|^{\text{approx,exact}}}{\left(1+\frac{1}{3}\overline{r}^2\right)}\\ f_m\left(\overline{r},\overline{h}\right) &= \frac{\overline{\dot{\gamma}}\left(\overline{r},\overline{h}\right)}{\left(1+\frac{1}{3}\overline{r}^2\right)}\end{aligned} \tag{A6}$$

Note that f_m is always exact in the present model. Moreover, note that

$$\lim_{\overline{\eta}\to 1}\overline{z}_c\left(\overline{\eta},\overline{r},\overline{h}\right)\Big|^{\text{approx, exact}} = \frac{1}{\overline{\dot{\gamma}}\left(\overline{r},\overline{h}\right)} \tag{A7}$$

ensures the continuity of the pressure gradient between the mono-viscous and the bi-viscous regions.

The pressure can be calculated as

$$\begin{aligned}p(r)|_{r>r_2} &= Cr_{max}\int_{\overline{r}}^{\infty} f_m\left(\overline{r},\overline{h}\right)d\overline{r}\\ p(r)|_{r_1\le r\le r_2} &= Cr_{max}\left(\int_{\overline{r}}^{\overline{r}_2} f_b\left(\overline{\eta},\overline{r},\overline{h}\right)d\overline{r}+\int_{\overline{r}_2}^{\infty} f_m\left(\overline{r},\overline{h}\right)d\overline{r}\right)\\ p(r)|_{r<r_1} &= Cr_{max}\left(\int_{\overline{r}}^{\overline{r}_1} f_m\left(\overline{r},\overline{h}\right)d\overline{r}+\int_{\overline{r}_1}^{\overline{r}_2} f_b\left(\overline{\eta},\overline{r},\overline{h}\right)d\overline{r}+\int_{\overline{r}_2}^{\infty} f_m\left(\overline{r},\overline{h}\right)d\overline{r}\right)\end{aligned} \tag{A8}$$

where, for sake of simplicity, the labels for *exact* and *approximated* results have not been indicated here. The coordinates $\overline{r}_1$ and $\overline{r}_2$ can be written as

$$\overline{r}_1 = \left[\mathcal{Q}-\sqrt{-3-\mathcal{Q}^2+4\overline{\dot{\gamma}}_m\left(\overline{h}\right)\frac{1}{\mathcal{Q}}}\right],\qquad \overline{r}_2 = \left[\mathcal{Q}+\sqrt{-3-\mathcal{Q}^2+4\overline{\dot{\gamma}}_m\left(\overline{h}\right)\frac{1}{\mathcal{Q}}}\right] \tag{A9}$$

where

$$\mathcal{Q} = \sqrt{-1+\frac{1}{\mathcal{P}}+\mathcal{P}},\qquad \mathcal{P} = \sqrt[3]{-1+2\left(\overline{\dot{\gamma}}_m\left(\overline{h}\right)\right)^2+2\overline{\dot{\gamma}}_m\sqrt{\left(\overline{\dot{\gamma}}_m\left(\overline{h}\right)\right)^2-1}} \tag{A10}$$

and $\overline{\dot{\gamma}}_m\left(\overline{h}\right) = \overline{\dot{\gamma}}(1,\overline{h})$.

The lubrication force can be finally obtained by integration of the pressure on $\overline{r}$ variable (see Eq. (26)). An inspection of Eqs. (A8) allows us to conclude that the relative error of the force defined as

$$\text{err} = \left|1-\frac{F^{approx}}{F^{exact}}\right| \tag{A11}$$

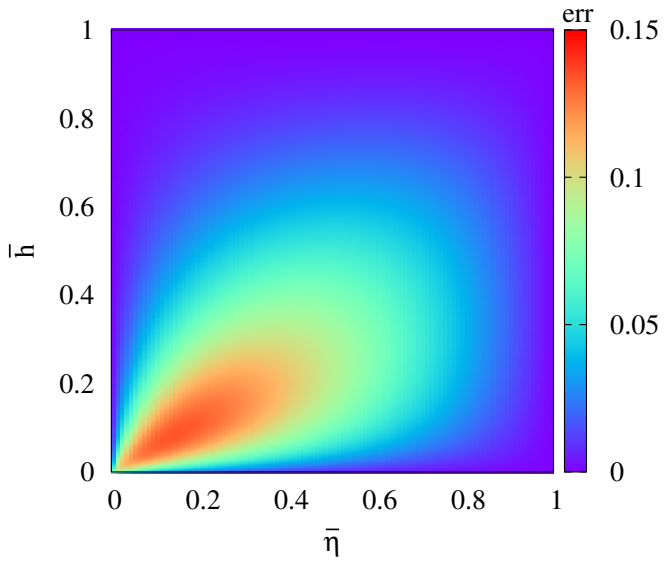

FIG. 12. Error of the model lubrication force between two particle as a function of the dimensionless parameters.

depends only on the two variables: $\overline{\eta}$ and $\overline{h}$.

The errors in the calculation of the force for distances smaller than h_0^{lim} (at larger distances the error is null) have been calculated numerically. The result is displayed in Fig. 12, where it is clear that the greatest errors are present for small values of both $\overline{\eta}$ and $\overline{h}$. It is worth to notice that the maximum relative error obtained is bounded and always below 0.14.

Appendix B: Reynolds number in the boundary layer for $\eta_1 \to 0$

When the limit $\eta_1 \to 0$ is considered, there are two competing effects affecting the Reynolds number in the low viscosity regions. On one hand, the Reynolds number increases as consequence of the reduction of the viscosity. On the other hand, the width of the low-viscosity layer decreases, becoming infinitesimal (See Sec. IV C) in the limit above, therefore contributing to diminish the local Reynolds number. In this Appendix we demonstrate that the Reynolds number associated to the low viscosity region tends to a finite value in the limit of $\eta_1 \to 0$.

Let us define a local Reynolds number $\mathrm{Re}(r)|_b$ dependent on r

$$\mathrm{Re}(r)|_b = \frac{\rho L_1(r) V_1(r)}{\eta_1} \tag{B1}$$

where $r_1 < r < r_2$. L_1 and V_1 are the typical length and velocity scales for the layer of liquid with viscosity η_1, which read

$$\begin{aligned} V_1(r) &= u(r, z_{max})|_b \\ L_1(r) &= \frac{h(r)}{2} - z_c(r) \end{aligned} \tag{B2}$$

where $u(r,z)|_b$ is defined at Eq. (10) and $z_{max} = (c(r) \pm z_c(r))$. When the limit $\eta_1 \to 0$ is taken, the next expression is obtained for the Reynolds number

$$\lim_{\eta_1 \to 0} \mathrm{Re}(r)|_b = \frac{3}{4}\frac{\rho r V}{\eta_0}\left(\frac{\dot{\gamma}_c h^2(r)}{3rV} - 2 + \frac{3rV}{\dot{\gamma}_c h^2(r)}\right) \tag{B3}$$

where V is the velocity of the particle. Similar to standard lubrication analysis for a mono-viscous fluid, as long as this finite value remains small in the interval $r \in (r_1, r_2)$, the low Reynolds approximation will be valid for the case $\eta_1 \to 0$.